*Egypt. J. Chem.* **Vol. 64,** No. 3 pp. 1395 - 1409 (2021)

# Egyptian Journal of Chemistry

**http://ejchem.journals.ekb.eg/**

## Preparation and Characterization of Novel Zinc Aluminate Nano-Powders Doped with Copper (II), Loaded and Non-loaded with Carbon Spheres Using Co- Precipitation Method and Its Environmental Application

**Mohamed A. Zayed^1, Mohamed M. Rashad [2], Diaa Ryan[2], Shimaa M. [1]**

[1] *Chemistry Department, Faculty of science, Cairo University, 12613 Egypt.*

[2] *Central Metallurgical Researches and Development Institute, Cairo Egypt*

**Abstract**

Due to rapid industrialization, the presence of heavy metals in water and wastewater is a matter of environmental concern. Though some of the metals are essential for our system but if present beyond their threshold limit value (TLV), they are harmful and their treatment prior to disposal becomes inevitable. The present communication has been addressed for the removal of Cr (VI) from aqueous solutions by synthesized zinc aluminate novel nano-materials doped with copper (II); loaded and non-loaded with carbon spheres (CSs) using the co-precipitation technology. The as-prepared precursors of $Cu(x)Zn(1-x)Al_2O_4$ were annealed at 1000 $^oC$ for 2 h. The characterization of the samples nanoparticles were implemented by X-ray fluorescence (XRF), X-ray diffraction (XRD), transmission electron microscopy (TEM) analysis, photoluminescence spectra (PL) as well as the optical properties was demonstrated by UV–visible–near IR spectrophotometer. The optical properties of the prepared nano-materials and their catalytic performances are well discussed. Batch experiments were adopted for the adsorption of Cr (VI) from its solutions. The effect of doped copper ions and Cu (II) / CSs co-dopants on the behavior of $ZnAl_2O_4$ on removal of chromium was studied using inductively coupled plasma (ICP) analysis that had been used to measure removed and remaining Cr (VI) from its water polluted samples.

*Key Words*: Zinc Aluminate, copper (II) and Cu (II)/CSs co-dopants, Co-precipitation, XRF, XRD, TEM, Photoluminescence (PL), Cr (VI) removal.

### 1.Introduction

Transition metal-oxide spinels are important in many application fields because of their high chemical and thermal stability, high mechanical resistance, hydrophobicity, and low surface acidity (Zawadzki M. 2001, Wrzyszcz J. 2002 and Nilsson M. 2009) [1-3]. They are being suitable for a wide range of applications, such as optical coating or host matrix, high temperature ceramic material, catalyst and catalyst support (Tzing WS. 1996, Phani AR 2001 and Zawadzki M. 2001) [4-6]. Among the most interesting materials of that kind, zinc aluminate ($ZnAl_2O_4$), with spinel structure belonging to Fd3m space group , offers many advantages, $ZnAl_2O_4$ is one of the best wide band gap compound semiconductor (Eg = 3.8 eV) (Chen XY. 2011)[7] for various optoelectronic applications (Li X. 2011)[8] and electronic and optical materials. Zinc aluminates were used also in photo-electronic devices, electroluminescence displays, stress imaging devices, and highly efficient phosphors. In recent years, $ZnAl_2O_4$ spinel has been largely used as catalyst in several reactions such as degradation of gaseous toluene (Galetti AE. 2010) [9], ethanol steam reforming (Lenarda M. 2007) [10], combustion of soot under $NOx/O_2$ atmosphere (Zawadzki M. 2009)

*Corresponding author e-mail: mazayed429@yahoo.com; (Tel: 002-01005776675).
Receive Date: 25 November 2020, Revise Date: 06 December 2020, Accept Date: 12 December 2020
DOI: 10.21608/EJCHEM.2020.51062.3045

[11], isobutane combustion (Staszak W. 2010) [12], and the transesterification (Pugnet V. 2010) [13] of waste frying oil (WFO) with methanol and ethanol was studied in a batch reactor using a zinc aluminate catalyst, prepared by the combustion reaction method. The reaction runs were carried out for 2 hours, using alcohol: oil molar ratio of 40:1, temperature range of 60–200 °C, catalyst ratio of 1–10% wt., using 700 rpm stirring. Spinel $ZnAl_2O_4$ semiconductors have been synthesized using a variety of different methods, such as the solid-state reaction method (Zou, L. 2006 and Van der Laag 2004) [14, 15] and a self-generated template pathway (Zou, L. 2006) [14], the combustion method (Ianos, R. 2012) [16], the sol–gel method (Wei X. 2006) [17] and a co-precipitation approach (Cheng B C. 2013) [18], were also employed. The polymeric precursor method (Gama L. 2009) [19], the citrate precursor method (Li X. 2011) [20], a hydrothermal process (Zhu, Z. R 2012) [21], a solvent-thermal approach (Fan G. L 2011) [22], and the microwave-hydrothermal route (Zawadzki M. 2009) [11] had been employed. Several doped $ZnAl_2O_4$ compounds, were described how the materials properties can be improved according to the dopants or the doping methods as explained in previously published research papers [23-27]. The present paper, $Cu(x)Zn(1-x)Al_2O_4$ nanoparticles have been synthesized by co-precipitation where x (0.2, 0.4, 0.6, 0.8 and 1.0). Then loaded the prepared nanoparticles with CSs. $Cu(x)Zn(1-x)Al_2O_4$ nanoparticles loaded and non-loaded with CSs were investigated to check the change in phase structure and crystallite sizes of the newly prepared spinels. Also their optical properties and their behavior toward the removal of Cr (VI) from its polluted sample solutions were studied.

## 2. Experimental

### *2.1. Materials*:

The chemicals used in this research are of the analytical grade. They included aluminum chloride hexahydrate ($AlCl_3.6H_2O$ 98%, 241.45 g $mol^{-1}$, Loba. Chemie). Zinc chloride ($ZnCl_2$ 97%, 136.286 g $mol^{-1}$ Loba Chemie) and copper chloride ($CuCl_2$ 98%, BDH chemical Ltd.). They also included sucrose ($C_{12}H_{22}O_{11}$ 99.5%, 342.30 g $mol^{-1}$, Sigma-Aldrich) as a source of carbon spheres, ammonium carbonate ($(NH4)_2CO_3$ 99.9%, 96.09 g $mol^{-1}$, Sigma-Aldrich) as a reagent and potassium dichromate ($K_2Cr_2O_7$ 99.0%, 294.18 g $mol^{-1}$, Sigma-Aldrich) as a source of hexavalent chromium. Hydrochloric acid (HCl) (M.wt = 36.46 g $mol^{-1}$) with purity 30-34 % was purchased from ADWIC. The distilled water used in all preparations usually collected from all glass equipment.

### *2.2. Solutions*

A solution of 0.1 M Zinc chloride $ZnCl_2$ (> 97% purity) (M.wt = 136.286 g $mol^{-1}$), was prepared by dissolving the accurately weighed amount (1.36286g) in least amount of HCl (~1 ml) and the volume completed with distilled water to 100 mL in volumetric flask .

A solution of 0.1 M aluminum chloride hexahydrate $AlCl_3.6H_2O$ (> 98%) (M.wt = 241.45 g $mol^{-1}$) , was prepared by dissolving the accurately weighed amount (2.4145 g) in the appropriate volume of distilled water and the volume completed to 100 mL volumetric flask.

A solution of 2000 ppm from potassium dichromate was prepared by dissolving the accurately weighed amount (0.5g) in appropriate volume and then completed with distilled water in 250 mL volumetric flask.

### *2.3. Preparation Procedures for Nano-spinels*

#### *2.3.1. Synthesis of carbon spheres*

Carbon spheres (CSs) were prepared by one step process, where sucrose is the source of carbon then heated at 100oC for 24h.

#### *2.3.2. Synthesis of zinc aluminate doped with Cu(II) nanoparticles using co-precipitation method non- loaded with carbon spheres*

Zinc aluminate doped with copper ion was synthesized, by inserting the aqueous solution of zinc chloride ($ZnCl_2$ 97%) into aqueous solution of aluminum chloride hexahydrate ($AlCl_3.6H_2O$ 98%), no further purification, with molar ratios 1**:** 2 of Zn: Al. Then the previous mixture was mixed with aqueous solution of copper chloride ($CuCl_2$ 98%); which has molar ratios of 0.0, 0.2, 0.6, 0.8, and 1.0. Afterwards, ammonium carbonate solution added drop-wisely into the mixture with stirring under strong ultrasonic agitation until pH of the solution reached 7. The powder was filtered, washed with deionized water, and dried at 100 °C overnight. Finally, the dry precursors were thermally treated in static air in muffle furnace with maximum holding temperature 1000 ºC for 2 h at a rate of 4oC/min as given by scheme 1.

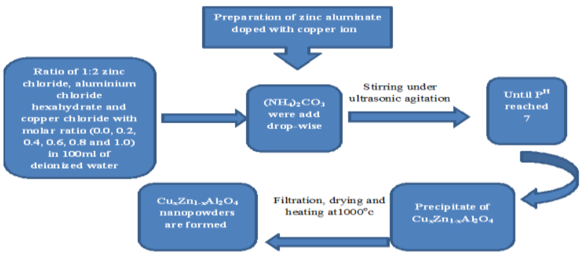


Scheme1: Synthesis of zinc aluminate doped with Cu (II) nanoparticles using co-precipitation method non-loaded with carbon spheres

**Table1** The theoretical and practical weight percentage of elements in $Cu_{(x)}Zn_{(1-x)}Al_2O_4$ nano-powder non-loaded with carbon spheres (CSs) doped with Cu (II) of x= 0.0, 0.2, 0.4, 0.6, 0.8, 1.0 using co-precipitation method and using XRF.

| | *Cu(II) ions molar ratio* | *Practical weight percentage (%)* | *Theoretical weight percentage (%)* |
|---|---|---|---|
| *Zn(II)* | **0.0** | **34.65** | **36.00** |
| | **0.2** | **28.00** | **28.85** |
| | **0.4** | **20.00** | **21.48** |
| | **0.6** | **15.15** | **14.35** |
| | **0.8** | **9.00** | **7.19** |
| | **1.0** | **0.01** | **0.00** |
| *Al(III)* | **0.0** | **28.00** | **29.43** |
| | **0.2** | **27.35** | **29.48** |
| | **0.4** | **30.00** | **29.54** |
| | **0.6** | **31.00** | **29.60** |
| | **0.8** | **28.00** | **29.66** |
| | **1.0** | **29.20** | **29.72** |
| *Cu(II)* | **0.0** | **0.14** | **0.00** |
| | **0.2** | **8.00** | **6.90** |
| | **0.4** | **15.40** | **13.9** |
| | **0.6** | **20.20** | **21.00** |
| | **0.8** | **29.00** | **27.95** |
| | **1.0** | **36.12** | **35.01** |
| *O(II)* | **0.0** | **37.21** | **34.91** |
| | **0.2** | **36.65** | **34.77** |
| | **0.4** | **34.60** | **35.08** |
| | **0.6** | **33.85** | **35.08** |
| | **0.8** | **34.00** | **35.20** |
| | **1.0** | **33.58** | **35.27** |

**Table 2** The XRF determined weight taken percentage and weight found of carbon spheres used for loading with zinc aluminate doped with Cu(II) nanoparticles ***synthesized*** by co-precipitation method.

| *Cu(II) ions molar ratio* | *Weight taken percentage (%)* **of CSs** | *Weight found percentage (%)* **of CSs** |
|---|---|---|
| **0.0** | 25.00 | 24.09 |
| **0.2** | 25.00 | 24.22 |
| **0.4** | 25.00 | 23.40 |
| **0.6** | 25.00 | 24.10 |
| **0.8** | 25.00 | 24.23 |
| **1.0** | 25.00 | 24.76 |

*2.3.3. Synthesis of zinc aluminate doped with Cu(II) nanoparticles using co-precipitation method loaded with carbon spheres*

The prepared $Cu_{(x)}Zn_{(1-x)}Al_2O_4$ nano-powder (x= 0.0, 0.2, 0.4, 0.6, 0.8, 1.0) from 2.3.2 were be added to carbon spheres, by grinding CSs with $Zn_{(1-x)}Cu_{(x)}Al_2O_4$ nano-powders (x= 0.0, 0.2, 0.4, 0.6, 0.8, 1.0) in proportions 25% of CSs and 75% of Zinc aluminate doped with Cu(II) nanoparticles for 20 min.

*2.4. Structure studies of the prepared nano-materials*

*2.4.1. X-ray fluorescence (XRF) study*

The X-ray fluorescence (XRF) is a powerful quantitative and qualitative analytical tool for elemental analysis of materials. Determination of the elements were carried out using X-ray fluorescence spectroscopy (XMDS 2726), with max.45 KV/ 50 μA.

*2.4.2. The X-Ray Diffraction (XRD) study*

XRD patterns of the resulting nano-powders were characterized by a Brucker D8-advance X-ray powder diffractometer CU K a radiation (k ¼ 1.5406 Å). The crystallite sizes of the produced zinc aluminate spinels were calculated from the most intense peak using Debyee Scharrer formula:

$$d_{RX} = \frac{K\lambda}{\beta}\ Cos\ 2\theta \qquad (1)$$

Where $d_{RX}$ is the crystallite size, k = 0.9 is a correction factor to account for particle shapes, $\beta$ is full width at half maximum (FWHM) of the most intense diffraction peak (3 1 1) plane, $\lambda$ is the wavelength of Cu target = 1.5406 $Å$, and $\theta$ is the Bragg angle at $2\theta$ = 35.42º which is strongest peak was used to calculate the average size of the nanoparticles.

*2.4.3. Morphology studies of the prepared spinels*

The micrographs of produced $Cu_{(x)}Zn_{(1-x)}Al_2O_4$ spinel samples were inspected by direct observation via high resolution transmission electron microscope (HR TEM; JEM-2100, Japan). HR-TEM samples were prepared by dispersing the powders in acetone. Ultrasonic oscillation for 1 h was introduced to decrease the aggregation followed by placing a drop of the suspension on holey carbon film supported on copper grids.

*2.4.4. Spectral measurements*

The UV-VIS absorption and diffuse reflectance spectrum of the prepared nano-materials were recorded at room temperature using UV-VIS-NIR spectrophotometer (Jasco-V-570 spectrophotometer, Japan) fitted with integrating sphere reflectance unit (ISN) in the wavelength range 200-2000 nm. Photoluminescence (PL) spectra were obtained at room temperature using fluorescence spectrophotometer (SHIMADZU RF-5301PC Japan) with xenon discharge lamp (150 *W*) as excitation source, at room temperature using an excitation wavelength equal to 200 nm.

*2.5. Environmental application of the prepared nano- spinels*

*2.5.1. Adsorption procedure:*

Removal of Cr(VI) from aqueous solutions of concentration 2000 ppm for 1 h in contact with 1 g nano-material samples during constant stirring. The amount of the adsorbed cation is obtained by difference of Cr (VI) concentration before and after adsorption by using ICP-AES. The percent removal = [Cr VI] after/ [Cr VI] before X 100.

*2.5.2. Measurements:*

To study, detect and measure removal of Cr (VI) from wastewater were inspected by inductively coupled plasma (ICP) with torch has a diameter 0.5-1.0 inch and magnetic field oscillates at 27.2 MHz typically argon gas is the plasma gas and nebulizer gas (with the sample) the formed plasma contains a high properties of cations and electrons and has electron density $10^{13}$- $10^{15}$ electrons/cm$^3$.

## 3. Results and discussion

Before going to investigate structure of the newly prepared nano-materials by co-precipitation method, the proposed general formulae ($Cu_{(x)}Zn_{(1-x)}Al_2O_4$) of these compounds should be proved by elemental analysis (EL) of its element constituents like Zn and Al together with the dopants Cu and Cu/CSs. Due to the insolubility of the prepared nan-powders; the used of X-Ray Fluorescence (XRF) is strongly recommended.

*3.1. Elemental Analyses (EA) by X-Ray Fluorescence (XRF)*

The calculated theoretical and practical weight percent's of constituent elements of the novel prepared Cu(x)Zn(1-x)$Al_2O_4$ nano-powder had been determined by XRF at different ratios of doped copper (x= 0.0, 0.2, 0.4, 0.6, 0.8, 1.0) and/or doped CSs are given in Tables (1 and 2)

*3.1.1. XRF of zinc aluminate substituted by Cu(II) nanoparticles synthesized by co-precipitation method non- loaded with carbon sphere*

From the data presented in **Table1**, it is clear that the calculated weight percent of the elements and practical found percent are correlated to each other; which means that the formed nanoparticles have similar proportions without any contaminations. These data confirm the proposed general formulae of the newly prepared zinc aluminate doped with Cu(II); $Cu_{(x)}Zn_{(1-x)}Al_2O_4$ nano-powder at different ratios x= 0.0, 0.2, 0.4, 0.6, 0.8, 1.0 and proved its correct proportions.

*3.1.2. XRF determined carbon spheres used for loading zinc aluminate doped with Cu(II) nanoparticles and synthesized by co-precipitation method*

The data presented in **Table2** refer to a good correlation between theoretical and practical data of CSs%; and found to be close to 25%, so the proportions of CSs and zinc aluminate doped with Cu (II) nanoparticles are closely 25% to 75% respectively. These data also confirm the successful insertion of carbon spheres in the entity of the prepared nanomaterials obtained by co-precipitation technique at different doped Cu(II) ratios.

*3.2. XRD used for identification of structural formulae of zinc aluminate nanoparticles doped with Cu (II) and/or with carbon spheres (CSs) using different techniques:*

*3.2.1. X- ray diffraction analysis of carbon spheres (CSs) non-loaded zinc aluminate*

XRD data of profiles of $Cu_{(x)}Zn_{(1-x)}$ $Al_2O_4$ (x =0.0, 0.2, 0.4, 0.6, 0.8 and 1.0 molar ratios) synthesized by co-precipitation method and non-loaded with carbon spheres are shown in Table 3 and in **Fig**.1.

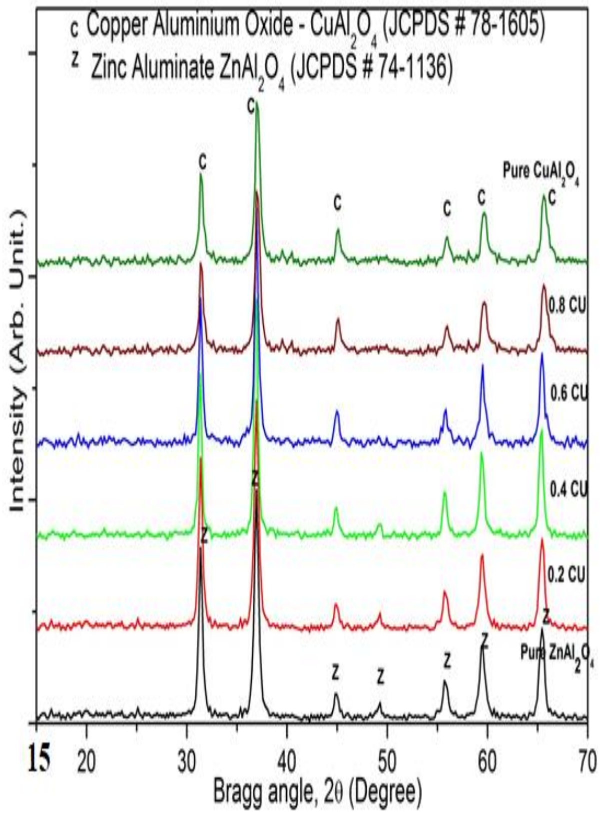


**Fig 1**: XRD patterns of $Cu_{(x)}Zn_{(1-x)}$ $Al_2O_4$ (*x* from 0.0 to 1.0 molar ratios) annealed at 1000 °C for 2 h using co-precipitation

**Table 3:** Variation of crystallite size, Bragg angle, lattice parameter, unite cell volume and X-ray theoretical density of $Cu_{(x}$ $Zn_{(1-x))}Al_2O_4$ where x 0.0, 0.2, 0.4, 0.6, 0.8, 1.0 molar ratios annealed at 1000°C for 2 h using co-precipitation method non-loaded with CSs

| *Cu(II) ions molar ratio* | *Cry. Size (nm)* | **Bragg angle** *(2θ)* | *Lattice parameter (Å)`* | *Unite Cell volume (Å³)* | *X-ray theoretical density ρ (g/cm³)* | **Optical band gap energy** *(eV)* |
|---|---|---|---|---|---|---|
| 0.0 | 23.4 | 36.957 | 8.0606 | 523.7220 | 4.6507 | 3.58 |
| 0.2 | 25.2 | 36.954 | 8.0613 | 523.8643 | 4.6556 | 2.28 |
| 0.4 | 30.7 | 36.893 | 8.0740 | 526.3446 | 4.6090 | 2.24 |
| 0.6 | 23.7 | 36.951 | 8.0620 | 523.9871 | 4.6204 | 2.21 |
| 0.8 | 20.2 | 36.829 | 8.0877 | 529.0125 | 4.5672 | 2.16 |
| 1 | 37.4 | 36.998 | 8.0519 | 522.0366 | 4.6189 | 2.02 |

**Fig. 1** shows the XRD diffraction profiles of Cu ion doped in $Cu_{(x)}Zn_{(1-x)}$ $Al_2O_4$ (x =0.0, 0.2, 0.4, 0.6, 0.8 and 1.0 molar ratios) synthesized by co-precipitation method. It can be seen that the prepared nano-materials are present in single phase. The peaks are belonging to cubic structure with space group *Fd-3m* (JCPDS card # 74-1136) for $ZnAl_2O_4$ phase and (JCPDS card # 78-1605) for $CuAl_2O_4$. Also the figure shows that right shift after increasing copper percentage.

In **Table 3** the crystallite size of zinc aluminate doped with cupper by using co-precipitation method show a slightly change in their values due to the similarity in properties between copper and zinc. The lattice parameter ''a'' of the samples was calculated using the following equation

$$d_{hkl} = \frac{a}{\sqrt{h^2+k^2+l^2}} \quad (2)$$

Where *a* is the lattice parameter, *d* is the inter-planar distance and (*hkl*) are the Miller indices. The values of lattice parameter and unit cell volume are listed in Table 3. The X-ray theoretical density was estimated using the following equation

$$\rho_X = \frac{\sum A}{N_A V} \quad (3)$$

Where $\rho_X$ is the X-ray theoretical density, *A* is sum of the atomic weights of all the atoms in the unit cell, *V* is the volume of the unit cell and *NA* is the Avogadro's number. It can be seen that the lattice parameter (*a*) and unit cell volume were slightly changed by addition of copper to zinc aluminate.

### 3.2.2. *XRD of Zinc aluminate doped with Cu(II) Nano-particles loaded with carbon spheres (CSs) synthesized by co-precipitation method*

XRD diffraction profiles of $Cu_{(x)}Zn_{(1-x)}$ $Al_2O_4$ (x =0.0, 0.2, 0.4, 0.6, 0.8 and 1.0 molar ratios) synthesized by co-precipitation method loaded with carbon spheres shown in Table 4 and in **Fig2.**

From **Fig.2**, it can be seen that single phase of $Cu_{(x)}Zn_{(1-x)}$ $Al_2O_4$ (x =0, 0.2, 0.4, 0.6, 0.8 and 1.0). The peaks were belonging to cubic structure with space group *Fd-3m* (JCPDS card # 74-1136) for $ZnAl_2O_4$ phase and (JCPDS card # 78-1605) for $CuAl_2O_4$. Also the figure shows that right shift after increasing copper percentage. After zinc aluminate doped with Cu(II) and loaded with CSs; the crystallite size is decreasing from 23.4 to 15.09 for pure zinc aluminate and from 37.4 to 17.88 for pure copper aluminate as shown in **Table 4.** It is observed in **Fig.2,** the peaks become boarder than in **Fig.1.** The data obtained from applying the Scherrer equation (Table 4) and full width at half maximum method; it stems that the crystallites become quite small such as non-uniform distortion of the lattice, crystallographic defects, the extensive presence of the dislocations and high levels of residual stress in the structure of the material due to the presence of pores of the nature of its microstructure.

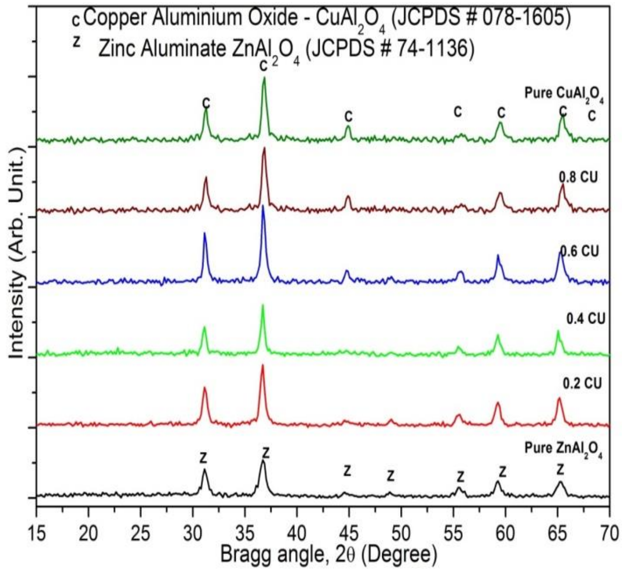


**Fig.2** XRD patterns of $Cu_{(x)}Zn_{(1-x)}$ $Al_2O_4$ (*x* from 0.0 to 1.0 molar ratios) using co-precipitation and loaded with carbon spheres

**Table 4:** Variation of crystallite size and optical band gap energy of $Cu_{(x)}$ $Zn_{(1-x)}Al_2O_4$ where *x* 0.0, 0.2, 0.4, 0.6, 0.8, 1.0 molar ratios annealed at 1000ºC for 2 h using co-precipitation method loaded with carbon spheres

| Cu(II) ions molar ratio | *Cry. Size (nm)* | Optical band gap energy *(eV)* |
|---|---|---|
| **0.0** | 15.09 | 2.55 |
| **0.2** | 17.21 | 2.19 |
| **0.4** | 17.48 | 1.99 |
| **0.6** | 16.65 | 1.97 |
| **0.8** | 14.61 | 1.85 |
| **1.0** | 17.88 | 1.83 |

### 3.3. *Morphology and microstructure*

The morphology of the prepared nano-materials had been studied by Field Emission Scanning Electron

Microscope (FE-SEM) and High Resolution Transmission Electron Microscopy (HRTEM).

*3.3.1. Field emission scanning electron microscopy (FE-SEM)*

The morphology of the synthesized carbon spheres was investigated by FE-SEM and the results are shown in **Fig.3**.

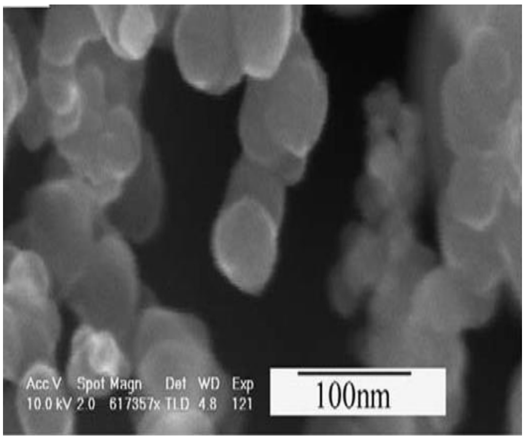


**Fig.3** FESEM micrographs of carbon sphere

The results in **Fig.3** certify that the carbon spheres have a spherical morphology (Zhuang Z.-H. 2009) [28] with good dispersed structure and highly homogeneous in size. The figure shows that the sizes of the carbon spheres ~ 60 nm; so when carbon spheres added to the nanoparticle (zinc aluminate substituted with copper ion) will form a nano-composite of good homogeneity.

3.3.2. *High Resolution Transmission Electron Microscopy (HR-TEM)*

The morphology of the prepared nano-material both loaded and non-loaded with carbon spheres (CSs) had been carefully investigated by the most efficient technology (HR-TEM). The results obtained are shown in Figs (4 and 5).

*3.3.2.1. HR-TEM of zinc aluminate doped with Cu(II) nanoparticles non-loaded with carbon spheres synthesized by co-precipitation method*

The morphology of zinc aluminate doped with Cu (II) nanoparticles non-loaded with carbon spheres synthesized by co-precipitation method is found to be homogeneous and spinel particles with cubic structure consist of uniform quasi-spherical crystallites of an average size ~ 25 nm in Fig.(4.a) for pure zinc aluminate. After doping with copper ions Fig.(4.b), Cu(II) inter to the lattice of zinc aluminate and form a new shell so the interspace and aggregation increase with copper and form a regular and uniform shape. Aluminum and copper agglomerated well which found in pure copper aluminates Fig.(4.c). The particle sizes of the prepared samples shown via HR-TEM are very close to the detected values obtained from the XRD measurements.

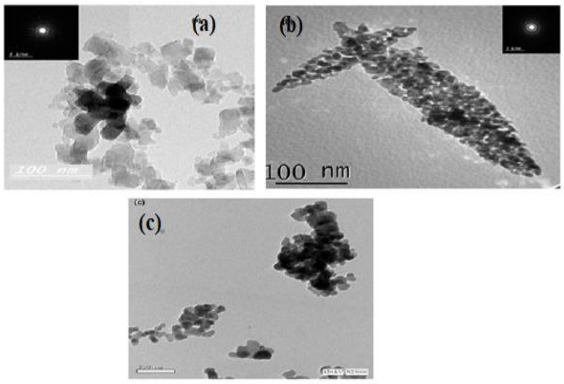


**Fig.4.HR-TEM micrographs for $Cu_{(x)}Zn_{(1-x)}$ $Al_2O_4$ where a) x is 0.0, b) x is 0.6 molar ratios and c) x is 1.0 molar ratios annealed at 1000ºC for 2 h using co-precipitation method not loaded with carbon spheres**

3.3.3. *HRTEM of zinc aluminate doped with Cu(II) nanoparticles loaded with carbon spheres synthesized by co-precipitation method*

The HR-TEM micrographs of **$Cu_{(x)}Zn_{(1-x)}$ $Al_2O_4$** (x=0.0, 1.0) loaded with carbon spheres are shown in **Fig.(5.a, b).**

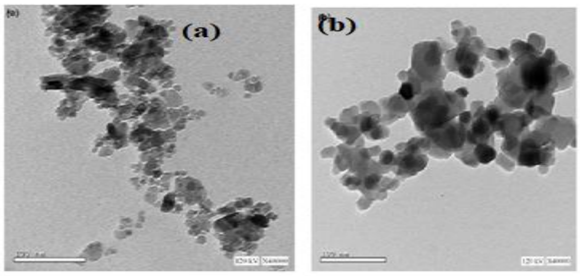


**Fig.5.HR-TEM micrographs for $Cu_{(x}$ $Zn_{(1-x))}Al_2O_4$ where a) x is 0.0, b)x is 1.0 molar ratios using co-precipitation method loaded with carbon spheres**

Fig. 5 results show that; the morphology is homogeneous and spinel particles with cubic structure consist of a spherical crystallites of an average size ~ 15 nm in **Fig.(5.a)** for pure zinc aluminate which is very small and copper aluminate has a crystal size ~ 18 nm **Fig.(5.b)**, which equivalent to XRD data. These micrographs give an indication that there is a great combination between CSs and spinal moiety; which cause the decreasing in the crystal size.

### *3.4. Optical properties*

Among the most interesting materials of that kind, zinc aluminate ($ZnAl_2O_4$), with spinel structure belonging to Fd3m space group , offers many advantages, $ZnAl_2O_4$ is one of the best wide band gap compound semiconductor (Eg = 3.8 eV) (Chen XY. 2011)[7] for various optoelectronic applications (Li X. 2011)[8] and electronic and optical materials. Zinc aluminates were used also in photo-electronic devices, electroluminescence displays, stress imaging devices, and highly efficient phosphors. Consequently the study of optical properties and semiconducting ability of the newly prepared Zinc aluminate doped with Cu (II) and co-doped with Cu (II)/CSs via energy gap calculation from their optical properties is very important to confirm its possible practical applications. The applied techniques are UV-VIS-NIR and photoluminescence spectroscopy (PL).

### *4.2.1. UV-VIS-NIR Spectra of zinc aluminate doped with Cu(II) nanoparticles synthesized by co-precipitation method and non-loaded with carbon spheres*

UV-VIS-NIR Spectra of zinc aluminate doped with Cu(II) nanoparticles synthesized by co-precipitation method non-loaded with carbon spheres are shown in Figs.6 and 7.

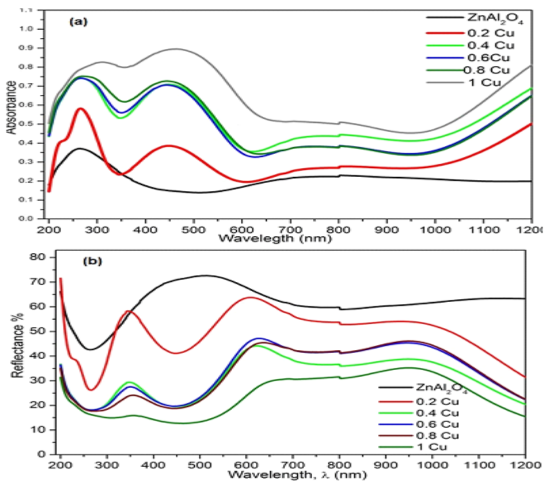


**Fig.6: (a) Absorbance (b) Reflectance of $Cu_{(x)}Zn_{(1-x)}Al_2O_4$, nano-powders (where $x$ = 0.0,0.2, 0.4, 0.6, 0.8, 1.0) , using co-precipitation method non-loaded with CSs**

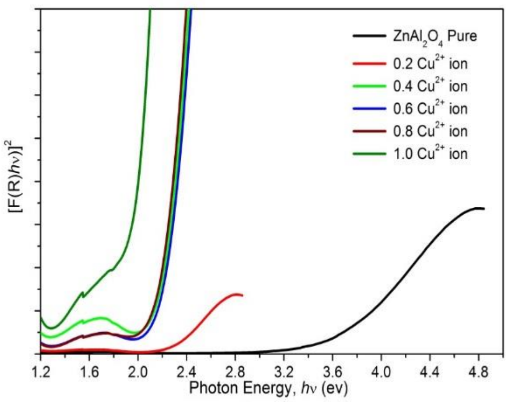


**Fig.7 Optical energy gap of $Cu_{(x)}Zn_{(1-x)}$ $Al_2O_4$, nano-powders (where $x$ = 0.0 to 1.0) by using co-precipitation method non-loaded with CSs**

The results of the recorded absorbance (A) revealed characteristic peaks of Al and Cu ions. The absorbance of 35% of pure zinc aluminate increases with increasing copper ratios until it reaches 85% in case of pure copper aluminate at x = 1.0 (**Fig.6**). From these results energy gap (Eg) in the structures of these nano-materials the absorption (A) is converted to the absorption coefficient ($\alpha$) using the following relation.

$$\alpha\,(v) = (1/d)\ \text{In}\ (I_o/I) = (100-R)/(2R) \quad (4)$$

Where ln (Io/I) is the absorbance (A) and d is the thickness of the sample. The reflectivity R can be transformed into a value proportional to the absorption using the Kubelka– Munk function:

$$(h\nu \boldsymbol{F}(R\infty))^n = A\,(h\nu - E_g) \quad (5)$$

The obtained results of the calculated band gap energy are represented in Fig.7; of the prepared $Cu_{(x)}Zn_{(1-x)}Al_2O_4$ (where x= 0.0, 0.2, 0.4, 0.6, 0.8 and 1.0) spinel nanoparticles without carbon spheres was estimated by extrapolating the linear portion of Tauc's plot to $(h\nu \boldsymbol{F}(R\infty))^n$ versus photon energy ($h\nu$) (n=2, for a direct band gap material). The optical band gap energy values (**Table 3) are** reduced from 3.58 eV for pure $ZnAl_2O_4$ **to** 2.02 for pure $CuAl_2O_4$ by increasing the molar ratio x = 0.0 to 1.0 of Cu(II).

### **4.1.UV-VIS-NIR Spectra of zinc aluminate doped with Cu(II) nanoparticles synthesized by co-precipitation method loaded with carbon spheres**

The results obtained of UV-VIS-NIR Spectra of Cu(x)Zn(1-x) $Al_2O_4$ (x =0, 0.2, 0.4, 0.6, 0.8 and 1.0) loaded with carbon spheres are shown in Figs.8 and 9.

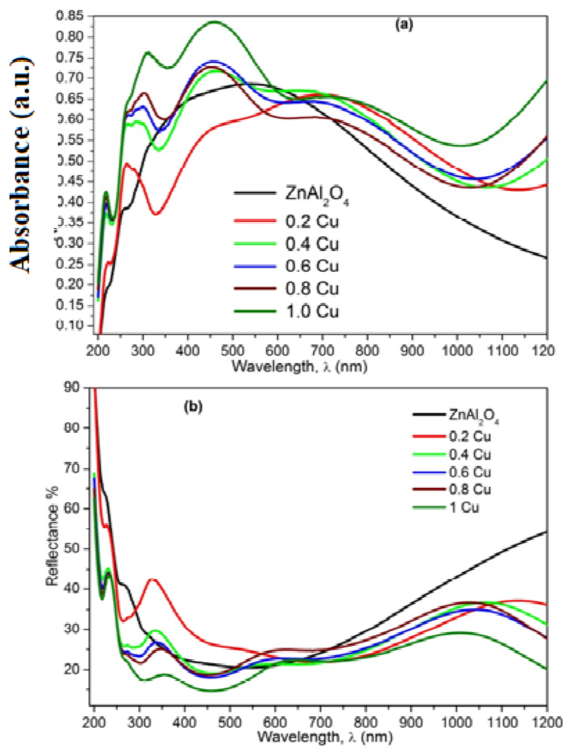


**Fig.8. (a)** Absorbance **(b)** Reflectance of **Cu*(x)*Zn*(1-x)* $Al_2O_4$** nano-powders (where *x* = 0.0,0.2, 0.4, 0.6, 0.8, 1.0), using co-precipitation method loaded with carbon spheres

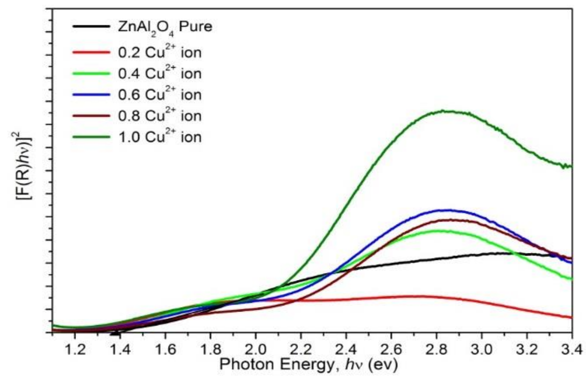


**Fig.9 Optical energy gap of Cu*(x)*Zn*(1-x)* $Al_2O_4$, nano-powders(where *x* = 0.0 to 1.0) using co-precipitation method loaded with carbon spheres**

These results revealed that; after binding Cu*(x)*Zn*(1-x)* $Al_2O_4$ (x =0, 0.2, 0.4, 0.6, 0.8 and 1.0) loaded with carbon sphere, there is an increase in the absorbance of pure zinc aluminate from 35% to 68%; which related to carbon sphere, however the absorbance of pure copper aluminate is still 85% (**Fig.8a)**. These results are used for calculation of energy gap values ($E_g$) according to equations (4) and (5) and graphically represented in Fig. 9. These results revealed that; there is a noticeable change in the band gap of Cu*(x)*Zn*(1-x)* $Al_2O_4$ (x =0, 0.2, 0.4, 0.6, 0.8 and 1.0) with variation of percent of carbon sphere. The band gap decreases from 3.58 eV to 2.55 eV for pure zinc aluminate and from 2.02 eV to 1.83 eV for pure copper aluminate (**Table 4).**

### 4.3. Photoluminescence spectroscopy (PL)

Photoluminescence (PL) spectroscopy is a useful tool to evaluate the quality and to study the physical parameters of semiconductor materials. PL spectra were recorded to investigate the recombination phenomena in the samples. PL can study the emission spectrum and provide information about the crystal defects of semiconductor; which might be due to the oxygen vacancies. Additionally, it can find the wavelength which has the maximum emission for the sample (the material which has high emission then have high absorbance at this wavelength) **equation (3).** Energy Equation of Quantum Mechanics from the following equation

(Energy) $E=\frac{hC}{\lambda}$ (3)

Where ***h*** is Plank's Constant, ***C*** is Speed of light and $\boldsymbol{\lambda}$ is wavelength.
So; it is possible to obtain the information of sub-band gap defect states (Kurbanov S.S. 2010) [29] in materials; which can be influenced by the synthesis condition (Anand GT. 2013) [30].

#### *4.3.1. PL of zinc aluminate doped with Cu(II) nanoparticles synthesized by co-precipitation method and non-loaded with carbon spheres*

**Fig.10** represents the PL spectra of **Cu*(x)*Zn*(1-x)* $Al_2O_4$**, nano-powders (where *x* = 0.0, 0.2, 0.4, 0.6, 0.8, 1.0) non-loaded with carbon spheres are measured at room temperature recorded with 200 nm excitation wavelength.

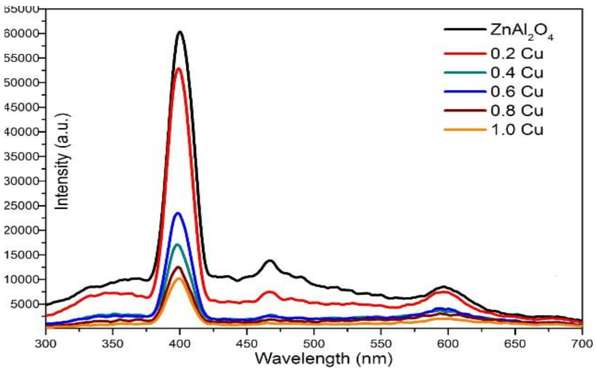


**Fig. 10 PL of Cu*(x)*Zn*(1-x)* $Al_2O_4$, nano-powders (where *x* = 0.0,0.2, 0.4, 0.6, 0.8, 1.0) by using co-precipitation method non-loaded with CSs**

In **Fig.10**, all samples show violet emission centered at about 400 nm (~3.10 eV) and exhibit weak broad luminescence bands with blue emission peak at 475 nm (~2.61 eV) and orange emission peak at 590-600 nm (~2.10 -2.07 eV). The emission peaks that occurred in the PL spectra of each metal aluminate samples are attributed to the recombination of electrons and photo-generated holes involving various structural defects, such as the ionized charge states of intrinsic defects, oxygen vacancies, metal (Zn, Cu) vacancy, metal interstitials, and oxygen antisites (Anand GT. 2010, than it T2019) [31, 32]. An electron in the valence band (VB) can be excited to higher energy levels in the conduction band (CB) and then falls to the conduction band maximum (CBM) through internal conversion (IC) and vibrational relaxation (VR). The electron at CBM can then radiatively recombine with a hole in the valence band or defect states in the band gap resulting in the violet, blue and orange light emissions. Therefore, the photoluminescence analysis of $ZnAl_2O_4$ nano-powders doped Cu(II) ions with different molar ratios exhibit interesting abilities for applications in violet, blue and yellow light-emitting devices.

*4.3.2.PL of zinc aluminate substituted by Cu(II) nanoparticles synthesized by co-precipitation method loaded with carbon spheres*

**Fig.11** shows the PL spectra of **Cu*(x)*Zn*(1-x)* $Al_2O_4$**, nano-powders (where *x* = 0.0, 0.2, 0.4, 0.6, 0.8, 1.0) loaded with carbon spheres measured at room temperature recorded with 200 nm excitation wavelength.

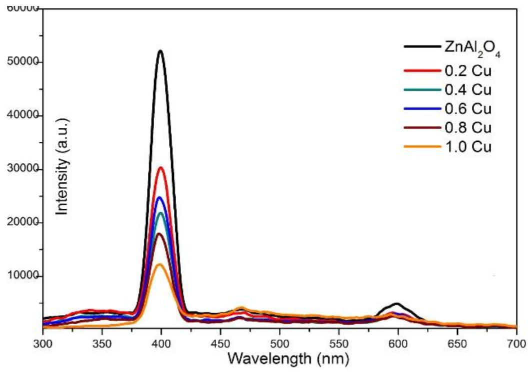


**Fig. 11.PL of Cu*(x)*Zn*(1-x)* $Al_2O_4$, nano-powders (where *x* = 0.0,0.2, 0.4, 0.6, 0.8, 1.0) using co-precipitation method loaded with carbon spheres**

There is no change in the PL spectra data after combination with carbon spheres. Fig.11 shows violet emission centered at about 400 nm (~3.10 eV) and exhibit weak broad luminescence bands with blue emission peak at 475 nm (~2.61 eV) and orange emission peak at 590-600 nm (~2.10 -2.07 eV). Also the intensity of the peaks decreases and become boarder so photocatalytic activity increases (jing L. 2006) [33].

Generally, also it is found that, the intensity decrease after doping with Cu(II) due to the inhibition of recombination of charge carriers and inducing geometrical distortion and creation of oxygen vacancy so during doping the energy levels increase so reducing the band gap Tables 5, 6 simultaneously decrease in the recombination rate of electron-hole due to which intensity decrease and peak are boarded that means low recombination of electron and holes give better photocatalytic activity (jing L. 2006) [33].

**4.4 Removal of Cr (VI) from aqueous solutions*)***

***4.4.1. Cr (VI) removal with Cu doped zinc aluminate nanoparticles non-loaded with carbon spheres.***

Chromium is an important strategic metal widely used in many fields due to its distinct properties (Lu D. 2017, Zadorozhnyy V.Y. 2014, Ma H. 2017, Zhao J. 2018, Xu X.-R. 2004) [34-38]. In the earth, chromium mainly exists in the oxidative states of hexavalent chromium and trivalent chromium. The chromium (III) compounds are relatively safe, stable, have low solubility and mobility. Chromium (VI) mainly exists as chromate ($CrO_4^{2-}$, $HCrO_4^{2-}$) and dichromate ($Cr_2O_7^{2-}$); which has high solubility. Due to hazardous contaminant (Nasseh N. 2017, Jyothi M.S. 2017) [39, 40] of chromium (VI), its removal has attracted much more attention, Such as physical methods, like adsorption (He X. 2017, Li S. 2017, Fu R. 2017, Ouyan X. 2017) [41–44], electrochemical (Zayed etal 2020) [45], and membrane filtration (Zhao J. 2018) [40], chemical precipitation (Peng H. 2018) [46], coagulation (Lu J. 2016) [47], and chemical reduction (Zhu Y. 2018, Yin W. 2017) [48,49] are often used to remove chromium (VI). Additionally, some biological treatments (Nhat-Thien N. 2018, Wei Y. 2017) [50, 51] and phytoremediation (Liu T. 2010) [52] are also applied to remove chromium (VI) in waste water and groundwater. Lead sulfate as a precipitation is used to precipitate chromium (VI) and it can remove chromium (VI) from 0.2 mol/L to 0.15 mmol/L, as shown in a recent study (Peng H. 2018) [51], but lead sulfate is a second pollutant, which is harmful for the environment. Recently, Chitosan can be used as an adsorbent for removal of Hexavalent Chromium, especially at low Cr (VI) concentrations (Dandhi G. 2018) [53], and other technology was applied (Zayed et al. 2020) [54].

In the present research zinc aluminate doped with Cu(II) and co-doped with Cu (II)/CSs in different molar ratios (0.0, 0.2, 0.4, 0.6, 0.8, 1.0) and prepared by co-precipitation method are used for removal of Cr(VI) pollutant from aqueous solutions containing 2000 ppm within limited time. The obtained results are presented in Tables 5 and 6.

**Table 5**: Variation of chromium (VI) using $Cu_{(x)}$ $Zn_{(1-x)}Al_2O_4$ where $x$ 0.0, 0.2, 0.4, 0.6, 0.8, 1.0 molar ratios annealed at 1000ºC for 2 h using co-precipitation method non-loaded with carbon spheres (CSs).

| ***Cu(II) ions molar ratio*** | ***Cr(VI) Remained (ppm)*** | ***Cr(VI) Remained %*** | ***Cr(VI) % Removed*** |
|---|---|---|---|
| **0.0** | 960 | 48.00 | 52.00 |
| **0.2** | 795 | 39.25 | 60.25 |
| **0.4** | 650 | 32.50 | 67.50 |
| **0.6** | 525 | 26.25 | 73.75 |
| **0.8** | 350 | 17.50 | 82.50 |
| **1.0** | 285 | 14.25 | 86.75 |

From the data represented in Table 5, it is clear that after doping of zinc aluminate nanoparticles with Cu(II) and the removal of Cr (VI) increases from 52% for zinc aluminate to 86.75% for copper aluminate. The highest removal of Cr(VI) is shown for $Cu_{0.2}Zn_{0.8}Al_2O_4$ (60.25 %) and $Cu_{0.8}Zn_{0.2}Al_2O_4$ reaches (82.5%) and 86.75% for pure copper aluminate at x = 1.0 respectively that attributed to the behavior and properties of copper over zinc. Therefore, $Cu_{(x)}Zn_{(1-x)}$ $Al_2O_4$, nano-powders (where $x$ = 0.0, 0.2, 0.4, 0.6, 0.8, 1.0) can be considered as an effective adsorbent to remove chromium (VI) ions from wastewater.

***4.4.2. Cr (VI) removal with Cu doped zinc aluminate nanoparticles loaded carbon spheres***

**Table 6**: Variation of chromium (VI) using $Cu_{(x}$ $Zn_{(1-x))}Al_2O_4$ where $x$ 0.0, 0.2, 0.4, 0.6, 0.8, 1.0 molar ratios annealed at 1000ºC for 2 h using co-precipitation method loaded with carbon spheres

| **Cu(II) ions molar ratio** | **Cr(VI) Remained (*ppm*)** | **Cr(VI) Remained %** | **Cr(VI) Removed %** |
|---|---|---|---|
| **0.0** | 911.57 | 45.78 | 54.22 |
| **0.2** | 594.40 | 29.72 | 70.28 |
| **0.4** | 338.60 | 16.93 | 83.07 |
| **0.6** | 207.80 | 10.39 | 89.61 |
| **0.8** | 195.50 | 9.75 | 91.25 |
| **1.0** | 95.30 | 4.77 | 95.23 |

The results represented in Table 6 it is clear that, after loading carbon spheres to zinc aluminates doped with copper ion, the nanoparticles become more active and the removal of Cr(VI) increases from 54.22% for pure $ZnAl_2O_4$ to 91.25% for doped Cu (II)/CSs Zinc aluminate at x = 0.8 and up to 95.23 for $CuAl_2O_4$ doped with CSs. This means that pure Zinc aluminate doped/co-doped $Cu_{(x}$ $Zn_{(1-x))}Al_2O_4$ and pure copper aluminate doped with CSs are highly effective in removal of Cr(VI) (95.23%) than those doped only with Cu (II) ions (86.23 %). Comparing these results with the obtained values in Table 4, it is clear that generally removal of Cr (VI) % with the prepared nanomaterials is increased in presence of CSs than without CSs; even pure Zinc aluminate doped with CSs (54.22%) and pure copper aluminate doped with CSs (95.23%).

## 5. Conclusions

The first part of this work is preparation of zinc aluminate doped with copper (II) of various molar ratios x = 0.0, 0.2, 0.4, 0.6, 0.8, 1.0 by co-precipitation method. By using XRF data in elemental analysis, the general formulae of the prepared nano-materials were proved via their elemental analyses. It is proved the correct ratios of zinc aluminate constituents doped with copper and Cu (II)/CSs co-dopant nanoparticles are formed. By studying the structure and morphology of the nanoparticles using XRD and HR-TEM they confirm a single phase with a homogenous and uniform structure having a cubic shape of $Cu_{(x)}$ $Zn_{(1-x)}Al_2O_4$ where *x* 0.0, 0.2, 0.4, 0.6, 0.8, 1.0. The optical properties were studied and from them it is obtained that the band gap decreases by addition of Cu(II). PL curves show that $Cu_{(x)}$ $Zn_{(1-x)}Al_2O_4$ where *x* 0.0, 0.2, 0.4, 0.6, 0.8, 1.0 can be used in violet, blue and yellow applications. It is found also, $Cu_{(x)}$ $Zn_{(1-x)}Al_2O_4$ where *x* 0.0, 0.2, 0.4, 0.6, 0.8, 1.0 nanoparticles are used as adsorbent to Cr(VI) from an aqueous solution to reach the maximum removal 86.75%. The second part is loading with CSs which prepared by one simple step method and verified by using FESEM. Here the effect of loading with CSs on $Cu_{(x)}$ $Zn_{(1-x)}Al_2O_4$ where *x* 0.0, 0.2, 0.4, 0.6, 0.8, 1.0 was studied. The cubic structure does not change by loading of CSs. The crystal size becomes very small. According to morphology, there is a good combination between $Cu_{(x)}$ $Zn_{(1-x)}Al_2O_4$ where *x* 0.0, 0.2, 0.4, 0.6, 0.8, 1.0 nanoparticles and CSs which cause the decreasing in crystal size and band gap. However, there is no change in PL curves. CSs enhance the effect of $Cu_{(x)}$ $Zn_{(1-x)}Al_2O_4$ where *x* 0.0, 0.2, 0.4, 0.6, 0.8, 1.0 nanoparticles on the removal of Cr(VI) from aqueous solution to reach the maximum removal 95.23%.

**Acknowledgement:** The authors acknowledge the supports of different measurements and explanations given by Chemistry Department, Faculty of Science, Cairo University, Metallurgy Research Institute Electronic and Magnetic Materials Department, and Institute of Petroleum Nanotechnology Department.

**Conflict of Interest:** Authors clarify no conflict of interest.

## Reference

[1] Zawadzki M, Miśta W and Kępiński L. Metal-support effects of platinum supported on zinc aluminate. *Vacuum*. 2001; 63:291-296.

[2] Wrzyszcz J, Zawadzki M, Trzeciak AM and Ziółkowski JJ. Rhodium complexes supported on zinc aluminate spinel as catalysts for hydroformylation and hydrogenation: preparation and activity. *Journal of Molecular Catalysis A: Chemical*.2002; 189:203-210.

[3] Nilsson M, Jansson K, Jozsa P and Pettersson LJ. Catalytic properties of Pd supported on $ZnO/ZnAl_2O_4/Al_2O_3$ mixtures in dimethyl ether auto thermal reforming. *Applied Catalysis B: Environmental*. 2009; 86:18-26.

[4] Tzing WS and Tuan WH. The strength of duplex $Al_2O_3$-
$ZnAl_2O_4$ composite. *Journal of Materials Science Letters*.1996; 15:1395-1396.

[5] Phani AR, Passacantando M and Santucci S. Synthesis and
characterization of zinc aluminum oxide thin fims by sol–gel technique. *Materials Chemistry and Physics*. 2001; 68:66-71.

[6] Zawadzki M, Wrzyszcz J, Strek W and Hreniak D.Preparation and optical properties of nano crystalline and nano porous Tb doped alumina and zinc aluminate. Journal of Alloys Compounds. 2001; 12:279-282

[7] Chen XY, Ma C, Zhang ZJ and Wang BN. Ultrafine gahnite ($ZnAl_2O_4$) nanocrystals: Hydrothermal synthesis and photoluminescent properties. *Materials Science and Engineering: B*. 2008; 151:224-230.

[8] Li X, Zhu Z, Zhao Q and Wang L. Photocatalytic degradation
of gaseous toluene over $ZnAl_2O_4$ prepared by different methods: A comparative study. *Journal of Hazardous Materials*. 2011; 186:2089-2096.

[9] Galetti AE, Gomez MF, Arrúa LA and Abello MC. Ni catalysts supported on modifid $ZnAl_2O_4$ for ethanol steam reforming.b*Applied Catalysis A: General*. 2010; 380:40-47.

[10] Lenarda M, Casagrande M, Moretti E, Storaro L, Frattini R and Polizzi S. Selective catalytic low pressure hydrogenation of acetophenone on $Pd/ZnO/ZnAl_2O_4$. *Catalysis Letters*. 2007; 114:79-84.

[11] Zawadzki M, Staszak W, Suárez FEL, Gómez MJI and López AB. Preparation, characterization and catalytic performance for soot oxidation of copper-containing $ZnAl_2O_4$ spinels. *Applied Catalysis A: General*. 2009; 371:92-98.

[12] Staszak W, Zawadzki M and Okal J. Solvothermal synthesis and characterization of Nano sized zinc aluminate spinel used in isobutane combustion. *Journal of Alloys and Compounds*. 2010; 492:500-507.

[13] Pugnet V, Maury S, Coupard V, Dandeu A, Quoineaud AA, Bonneau JL et al. Stability, activity and selectivity study of a zinc aluminate heterogeneous catalyst for the transesterification

of vegetable oil in batch reactor. *Applied Catalysis A: General*. 2010; 374:71-78.

[14] Zou, L., Li, F., Xiang, X., Evans, D. G. & Duan, X. Self-generated template pathway to high-surface-area zinc aluminate spinel with mesopore network from a single-source inorganic precursor. *Chem. Mater.* **.2006; 18,** 5852–585.

[15] Van der Laag, N.J., Snel, M.D., Magusin, P. C. M. M. & De With, G. Structural, elastic, thermophysical and dielectric properties of zinc aluminate ($ZnAl_2O_4$). *J. Eur. Ceram. Soc.2004;* **24,** 2417–2424.

[16] Ianos, R., Lazău, R., Lazău, I. & Păcurariu, C. Chemical oxidation of residual carbon from $ZnAl_2O_4$ powders prepared by combustion synthesis. *J. Eur. Ceram. Soc.2012;* **32,** 1605–1611.

[17] Wei, X. & Chen, D. Synthesis and characterization of nanosized zinc aluminate spinel by sol–gel technique. *Mater. Lett. 2006;* **60,** 823–827.

[18] Cheng, B. C., Ouyang, Z. Y., Tian, B. X., Xiao, Y. H. & Lei, S. J. Porous $ZnAl_2O_4$ spinel nanorods: high sensitivity humidity sensors. *Ceram. Int. 2013;* **39,** 7379–7386.

[19] Gama L. Synthesis and characterization of the $NiAl_2O_4$, $CoAl_2O_4$ and $ZnAl_2O_4$ spinels by the polymeric precursor's method. *J. Alloys Comp.2009;* **483,** 453–455.

[20] Li, X. Y., Zhu, Z. R., Zhao, Q. D. & Wang, L. Z. Photocatalytic degradation of gaseous toluene over $ZnAl_2O_4$ prepared by different methods: A comparative study. *J. Hazard. Mater.2011;* **186,** 208 –2096.

[21] Zhu Z. R. Photocatalytic performances and activities of $ZnAl_2O_4$ nanorods loaded with Ag towards toluene. *Chem. Eng. J*. 2012; **203,** 43–51.

[22] Fan G. L., Wang, J. & Li, F. Synthesis of high-surface-area micro/mesoporous $ZnAl_2O_4$ catalyst support and application in selective hydrogenation of o-chloronitrobenzene. *Catal. Commun.2011;* **15,** 113–117.

[23] Nirmala T. S. , Iyandurai N. , Yuvaraj S., Sundararajan M., Effect of $Cu^{2+}$ ions on structural, morphological, optical and magnetic behaviors of $ZnAl_2O_4$ spinel, Mater. Res. Express 7 (2020) 046104 https://doi.org/10.1088/2053-1591/ab7a7a

[24] Ramachandran S. Y., Selvam S.R., Sekhar A.C., Subramani D., Impact of $Mg^{2+}$ Ion on the Structural, Morphological, Optical, Vibrational, and Magnetic Behavior of Mg:$ZnAl_2O_4$ Spinel, https://doi.org/10.1007/s10948-019-05347-7

[25] Roniboss A.; Subramani A.; Ramamoorthy R.; Yuvaraj S.; Sundararajan M.; Dash C.S., Investigation of structural, optical and magnetic behavior of $MAl_2O_4$ (M= Zn and Co) nanoparticles via microwave combustion technique https://doi.org/10.1016/j.mssp.2020.105507

[26] Ramachandran S., Sekhar C., Dash D. C. S., Annadurai A. T., Thamilselvan M., Sundararajan S. M., Rapid Synthesis and Characterization of Pure and Cobalt Doped Zinc Aluminate Nanoparticles via Microwave Assisted Combustion Method, Journal of Nano-science and Nanotechnology, 20, 2382-2388, 2020 doi:10.1166/jnn.2020.17314

[27] Christina S. Y., Christina F. A., Sundararajan F. M., Sundararajan M., Palanisamy S., Hydrothermal synthesis of ZnO–CdS nanocomposites: structural, optical and electrical behavior, 46, 391-402, 2020 https://doi.org/10.1016/j.ceramint.2019.08.274

[28] Zhuang Z.-H. and Yang Z.-G. Preparation and Characterization of Colloidal Carbon Sphere/Rigid Polyurethane Foam Composites Journal of Applied Polymer Science, 2009; 114, 3863–3869.

[29] Kurbanov S.S., Igamberdiev Kh. T., Kang T.W. The UV-laser induced heating effect on photoluminescence from ZnO nanocrystals deposited on different substrates. J. Phys.D: Appl. Phys. 2010; 43.

[30] Anand GT, Kennedy LJ, Vijaya JJ. Microwave combustion synthesis, structural, optical and magnetic properties of $Zn_{(1-x)}Co_{(x)}Al_2O_4$ ($0\leq x\leq 0.5$) spinel nanostructures. *J Alloys Compd* 2013, **581**: 558–566.

[31] Anand GT, Kennedy LJ, Aruldoss U, *et al*. Structural, optical and magnetic properties of $Zn_{(1-x)}Mn_{(x)}Al_2O_4$ ($0\leq x\leq 0.5$) spinel nanostructures by one-pot microwave combustion technique. *J Mol Struct* 2015, **1084**: 244–253.

[32] Thanit T., Jiraroj T., Chanapa K. Effect of calcination temperature on structural and optical properties of $MAl_2O_4$ (M = Ni, Cu, Zn) aluminate spinel nanoparticles. *Journal of Advanced Ceramics 2019*, **8**(3): 352–366

[33] Jing L. and Sun J. Review of photoluminescence performance of nano-sized semiconductor materials and its relationships with photocatalytic activity. Solar Energy Materials and Solar Cells. 2006; 90, 1773-1787.

[34] Lu D., Yang M., Fang P., Li C. and Jiang L. Enhanced photocatalytic degradation of aqueous phenol and Cr(VI) over visible-light-driven

$Tb_xO_y$ loaded $TiO_2$-oriented nanosheets. Appl. Surf. Sci. **2017**, 399, 167–184.

[35] Zadorozhnyy V.Y., Klyamkin S.N., Zadorozhnyy M.Y., Bermesheva O.V. and Kaloshkin S.D.Mechanical alloying of nanocrystalline intermetallic compound TiFe doped by aluminum and chromium. J. Alloys Compd. **2014**, 586, S56–S60.

[36] Ma H., Zhou J., Hua L., Cheng F., Zhou L. and Qiao X. Chromium recovery from tannery sludge by bioleaching and its reuse in tanning process. J Clean Prod. **2017**, 142, 2752–2760.

[37] Zhao J., Liu M., Liang M., Ding B., Ding K. and Pan Y. OrganicsWastewater Degradation by a Mesoporous Chromium-Functionalized -$Al_2O_3$ with $H_2O_2$ Assistance. Water Air Soil Pollut. **2018**, 229, 135.

[38] Xu X.-R., Li H.-B., Li X.-Y. and Gu J.-D. Reduction of hexavalent chromium by ascorbic acid in aqueous solutions. Chemosphere **2004**, 57, 609–613.

[39] Nasseh N., Taghavi L., Barikbin B. and Khodadadi M. Advantage of almond green hull over its resultant ash for chromium(VI) removal from aqueous solutions. Int. J. Environ. Sci. Technol. **2017**, 14, 251–262.

[40] Jyothi M.S., Nayak V., Padaki M., Balakrishna R.G. and Soontarapa K. Eco-friendly membrane process and product development for complete elimination of chromium toxicity in wastewater. J. Hazard. Mater. **2017**, 332, 112–123.

[41] He X., Qiu X. and Chen J. Preparation of Fe(II)–Al layered double hydroxides: Application to the adsorption/reduction of chromium. Colloids Surf. A Physicochem. Eng. Aspects **2017**, 516, 362–374.

[42] Li S., Liu L., Yu Y., Wang G., Zhang H. and Chen A. $Fe_3O_4$ modified mesoporous carbon nanospheres: Magnetically separable adsorbent for hexavalent chromium. J. Alloys Compd. **2017**, 698, 20–26.

[43] Fu R., Zhang X., Xu Z., Guo X., Bi D. and Zhang, W. Fast and highly efficient removal of chromium (VI) using humus-supported nanoscale zero-valent iron: Influencing factors, kinetics and mechanism. Sep. Purif. Technol. **2017**, 174, 362–371.

[44] Ouyan X., Han Y., Cao X. and Chen J. Magnetic biochar combining adsorption and separation recycle for removal of chromium in aqueous solution. Water Sci. Technol. **2017**, 75, 1177–1184. 12.

[45] Zayed M.A., Mahmoud W. H. , Abbas A.A., Ali A.A. Mohamed G.G., A highly sensitive, selective and renewable carbon paste electrode based on a unique acyclic diamide ionophore for potentiometric determination of lead ions in polluted water samples, RSC Advances (RSC Adv.) 10, 17552 (2020).

[46] Peng H., Guo J., Li B., Liu Z. and Tao C. High-efficient recovery of chromium (VI) with lead sulfate. J. Taiwan Inst. Chem. Eng. **2018**, 85, 149–154.

[47] Lu J., Wang Z., Liu Y. and Tang Q. Removal of Cr ions from aqueous solution using batch electrocoagulation: Cr removal mechanism and utilization rate of in situ generated metal ions. Process Saf. Environ. Prot. **2016**.

[48] Zhu Y., Li H., Zhang G., Meng F., Li L. and Wu S. Removal of hexavalent chromium from aqueous solution by different surface-modified biochars: Acid washing, nanoscale zero-valent iron and ferric iron loading. Bioresour. Technol. **2018**, 261, 142–150.

[49] Yin W., Li Y., Wu J., Chen G., Jiang G., Li P., Gu J., Liang H. and Liu C. Enhanced Cr(VI) removal from groundwater by Fe0-$H_2O$ system with bio-amended iron corrosion. J. Hazard. Mater. **2017**, 332, 42 50.

[50] Nhat-Thien N., Lee S.-Y., Chen S.-S., Nguyen-Cong N., Chang C.-T., Hsiao S.-S., le T. T. K., C.-Y. Lin M.-F. and Wang L. Preparation of Zn-Doped Biochar from Sewage Sludge for Chromium Ion Removal.J. Nanosci. Nanotechnol. **2018**, 18, 5520–5527.

[51] Wei Y., Fang Z., Zheng L. and Tsang E.P. Biosynthesized iron nanoparticles in aqueous extracts of Eichhornia crassipes and its mechanism in the hexavalent chromium removal. Appl. Surf. Sci. **2017**, 399, 322–329.

[52] Liu T., Zhao L., Sun D. and Tan X. Entrapment of nanoscale zerovalent iron in chitosan beads for hexavalent chromium removal from wastewater. J. Hazard. Mater. **2010**, 184, 727–730.

[53] Dandhi G. and Sanja G. Evaluatihg the effectiveness of chitosan for removal of hexavalent chromium from wastewater. International Journal of Management Information. 2018, 3.2986

[54] Nahla Sayed Ismail, shimaa Mousa, Mohamed A. Zayed, Development of Carbon Paste Electrodes for the Selective Determination of Venlafaxine and its metabolite Desvenlafaxine in their Pure and Pharmaceutical Formulations Manuscript Egypt. J. Chem.2020, 63, 5, 27-28.

## عنوان البحث

**تحضير وفحص زنك الومينات مركبات نانو مستحدثة مخصبة بالنحاس الثنائي ومطعمة باجواء من الكربون باستخدام الترسيب المتضامن وتطبقاتها في التحاليل البيئية**

**المؤلفون :محمد عبد الجواد زايد , محمد محمد رشاد , ضياء ريان , شيماء محمود ابوعيطة**

## ملخص البحث

**لقد تم في هذا البحث تحضير وفحص مركبات زنك الوميناتفي صورة نانو مستحدثة مخصبة بالنحاس الثنائي ومطعمة باجواء من الكربون باستخدام الترسيب المتضامن والمعاملة الحرارية عند 1000 درجة مئوية لمدة ساعتين وتم دراسة تركيباتها باستخدم العديد من اجهزة الفحص من حيث التركيب الجزيئي بتحليل العناصر المكونه ونسبها بأستخدام جهاز XRF ووضع الضيغة التركيبية لها $Cu_{(x)}Zn_{(1-x)}Al_2O_4$ ثم دراسة الصيغة البنائية وطبيعة ترابط ذراتها بواسطة جهاز FT-IR وشكل اسطحها بواسطة أجهزة TEM ومعرفة حجم الجزيئات النانو المحضرة ودراسة شكلها البللوري بواسطة جهاز XRD وكذلك تم دراسة خواصها كمحفزات ونشاطها الضوئي بواسطة كل من الضوء العادي والأشعة فوق البنفسجية وكذلك أدائها مع الأنبعاث الضيائي photoluminescence spectra (PL) ومن ثم معرفة خواصها التحفيزية والضوئية ومن ثم امكانية استخدامها في تطبيقات عديدة وفعلا تم تطبقها في مجال ابحاث البيئة بأستخدامها في أزالة الكروم السداسي السام من بعض عينات المياة المحتوية علي هذا العنصر ومتابعة نسبة الأزالة المتغيرة بتغير صفات المركب المحضر بتغير نسب مكوناته وذلك بأستخدام جهاز بلازما الحث ICP-AES واثبتت النتائج نجاح التطبيق.**